UC Berkeley

Title

Predicting Excitation Energies of Twisted Intramolecular Charge-Transfer States with the Time-Dependent Density Functional Theory: Comparison with Experimental Measurements in the Gas Phase and Solvents Ranging from Hexanes to Acetonitrile.

Authors

Shee, James
Head-Gordon, Martin

Predicting excitation energies of twisted intramolecular charge-transfer states with time-dependent density functional theory: Comparison with experimental measurements in the gas-phase and solvents ranging from hexanes to acetonitrile

James Shee[*,†] and Martin Head-Gordon[*,‡,‡]

†Kenneth S. Pitzer Center for Theoretical Chemistry, Department of Chemistry, University of California, Berkeley, California 94720, USA

‡Chemical Sciences Division, Lawrence Berkeley National Laboratory, Berkeley, California 94720, USA

E-mail: jshee@berkeley.edu; mhg@cchem.berkeley.edu

Abstract

Electronically-excited states characterized by intramolecular charge-transfer play an essential role in many biological processes and optical devices. The ability to make quantitative *ab initio* predictions of the relative energetics involved is a challenging yet desirable goal, especially for large molecules in solution. In this work we present a data set of 61 experimental measurements of absorption and emission processes, both in the gas phase and solvents representing a broad range of polarities, which involve

intramolecular charge-transfer mediated by a non-zero, "twisted" dihedral angle between one or more donor and acceptor subunits. Among a variety of density functionals investigated within the framework of linear-response theory, the "optimally tuned" LRC-ωPBE functional, which utilizes a system-specific yet non-empirical procedure to specify the range-separation parameter, emerges as the preferred choice. For the entire set of excitation energies, involving changes in dipole moment ranging from 4 to >20 Debye, the mean signed and absolute errors are 0.02 and 0.18 eV, respectively (compared, e.g., to -0.30 and 0.30 for PBE0, 0.44 and 0.47 for LRC-ωPBEh, 0.83 and 0.83 for ωB97X-V). We analyze the performance of polarizable continuum solvation models available in Q-Chem that partition the solvent response into fast and slow time-scales, and clear trends emerge when measurements corresponding to the four small DMABN-like molecules and a charged species are excluded. We make the case that the large errors found only for small molecules in the gas phase and weak solvents cannot be expected to improve via the optimal tuning procedure, which enforces a condition that is exact only in the well-separated donor-acceptor limit, and present empirical evidence implicating the outsized importance for small donor-acceptor systems of relaxation effects that cannot be accounted for by linear-response TDDFT within the adiabatic approximation. Finally, we demonstrate the utility of the optimally tuned density functional approach by targeting the charge-transfer states of a large biomimetic model system for light-harvesting structures in Photosystem II.

Introduction

Excited states characterized by intramolecular charge-transfer (CT) from donor (D) to acceptor (A) subunits are ubiquitous in biological processes such as photosynthesis, chemical catalysis, and light emitting devices. Examples include the photoexcitation of chlorophyll dyes in Photosystem II, and band gap tuning of organic light emitting devices (OLEDs). An approach to increasing the efficiency of OLEDs involves a process known as thermally activated delayed fluorescence (TADF),[1,2] wherein facile interconversion of (dark) triplet states

to (bright) singlet excited states vastly increases quantum yields. However, an accurate description of the energetics of CT excited states, to date, remains challenging for *ab initio* methods.

Wavefunction methods aim to solve the Schrödinger equation in the space of electronically excited configurations, the size of which grows exponentially with the number of electrons if no approximations are made. Computationally tractable configuration interaction methods suffer from an inefficient description of dynamic electron correlation, and furthermore the required truncation at a low excitation level leads to a loss of size-consistency, which hinders reliable modelling of most chemical reactions. Alternatively, an exponential ansatz for the wavefunction containing a truncated heirarchy of excitation operators defines the size-consistent Coupled Cluster (CC) theory, and a subsequent linear response treatment yields a class of excited state methods known as Equation of Motion (EOM) CC. In the context of CT excitations, recent studies, e.g. Ref. 3, have found empirically that predictions accurate up to less than 0.1 eV require at least triple excitations. Bartlett and coworkers reach a similar conclusion via a theoretical argument, considering the following expression for the excitation energy, $EE = IP - EA - \frac{e^2}{R}$, where R denotes the D-A separation, and the ionization potential and electron affinity are defined as $IP = E(N-1) - E(N)$ and $EA = E(N) - E(N+1)$, where the number of electrons, N, equals the atomic number, Z. They put forth the concept of "charge-transfer separability", which asserts that for a D-A system at infinite separation, 1h and 2h1p excitations can be relevant for the ionized D subunit and 1p and 2p1h excitations for the A subunit, implying that proper treatment of the joint D-A system requires 3h3p excitations.[4] This situation is problematic, as EOM-CCSDT and EOM-CCSD(T) scale as $O(M^8)$ and $O(M^7)$, respectively, with system size. The effect of triples can be indirectly approximated with a similarity transformed (ST) variant of EOM-CCSD, which has been shown to yield accurate CT energetics at $O(M^5)$ cost.[4] Recent studies have reported that this can be further reduced by the back-transformed pair natural orbital STEOM-CCSD method, bt-PNO-STEOM-CCSD, at the expense of making

local correlation approximations.[5]

A further complication shared by wavefunction methods, which in fact is made more severe by their high-polynomial scaling, is the need to extrapolate to the complete basis set (CBS) limit in order to compare directly with experimental measurements. In principle, multiple calculations with finite basis sets of increasing size should be extrapolated to the CBS limit. However, this is simply infeasible for many medium to large sized molecules which exhibit CT excited states relevant, e.g., to biology and optical devices, and certainly adds unwanted hurdles to high-throughput screening projects. As a result, practitioners are often forced to rely on error cancellation and compute excitation energies with a triple-zeta basis set only, and have in many cases achieved reasonable accuracy with respect to experiments (with the exception of Rydberg states, which are highly sensitive to choice of basis set).[6–9]

A promising alternative to wavefunction approaches, which sidesteps the barriers due to both high scaling and extrapolation to the CBS limit, is exemplified by state-specific, orbital optimized methods for excited states such as ΔSCF[10,11] and the Restricted Open-Shell Kohn-Sham (ROKS) approach targeting open-shell singlets.[12–14] As will be discussed later in this work, the impressive accuracy often found empirically in the prediction of CT excitation energies suggests that the physical effect of correlated electronic reorganization in response to the newly created electron and hole need not be described by (expensive) theories that include triple excitations. In many cases, it appears that this effect can be accounted for, at least to some degree, by approaches in which the orbitals comprising the targeted excited state are allowed to variationally relax. However, ΔSCF and ROKS are reliable only when applied to excitations that are well-described by a single electronic configuration. While this is typically the case for most CT excited states, there are certainly exceptions which require superpositions of single excitations (e.g. the bis- and tri- PXZ-TRZ absorptions investigated presently). Furthermore, a rigorous theoretical foundation has yet to be established for methods such as ΔSCF and ROKS, due to the lack of a Hohenberg-Kohn theorem for excited states.[15]

The most popular alternative to wavefunction methods used to model a wide range of excited state properties is linear-response time-dependent density functional theory (TDDFT).[16–18] The favorable $O(M^{2-3})$ scaling enables its routine use even for very large system sizes, and accurate excitation energies directly comparable to experimental measurements have been reported using *only* double-zeta basis sets.[19–22] However, TDDFT is not without limitations, and has two main sources of error. The first stems from the adiabatic approximation,[17,23,24] which renders TDDFT unable to describe excited states characterized by double excitations or higher. The second involves a many-electron generalization of the self-interaction error known as "delocalization error".[25] Intuitively, this has to do with the tendency of DFT methods to overstabilize delocalized electronic states, illustrated most simply by the fractionally charged atoms predicted for stretched H_2^+.[26] Mathematically, delocalization error is manifested as the lack of a derivative discontinuity in the energy at integral electron numbers,[27] and a deviation from Janak's theorem[28] which implies straight-line behavior at fractional electron numbers.[29,30]

In particular, CT excitation energies calculated within TDDFT are very sensitive to the presence of delocalization error. This is most clearly understood in the limit of infinite separation between D and A subunits, where the vertical charge-transfer excitation energy is known exactly, i.e. $EE^{exact} = IP^D - EA^A$. Intuitively, when electrons are over-delocalized the predicted ionization potential is likely to differ from that observed experimentally. The TDDFT matrix equation, in this limit, yields[18] $EE^{TDDFT} = \epsilon_{LUMO}^A - \epsilon_{HOMO}^D$, where ϵ_{LUMO} and ϵ_{HOMO} are eigenvalues corresponding to the Lowest Unoccupied and Highest Occupied Molecular Orbitals of the Kohn-Sham (KS) system. It follows that $EE^{TDDFT} - EE^{exact} = \epsilon_{LUMO}^A - \epsilon_{HOMO}^D - IP^D + EA^A$,[27] from which it can be seen that, in the limit of infinitely separated D and A subunits, TDDFT will produce exact excitation energies when

$$\epsilon_{HOMO}^D = -IP^D \text{ and } \epsilon_{LUMO}^A = -EA^A. \tag{1}$$

In HF theory, Koopman's theorem guarantees both of these equalities, though only when the IP and EA are defined without orbital relaxation (e.g., the $N+1$ electron system is obtained by adding an electron into the LUMO of the N electron system, all else equal).[31] In contrast, Eq. 1 cannot be satisfied when LDA or GGA functionals are used, ultimately because the derivative discontinuity at integer values, defined as $\Delta_{xc} = v_{xc}^+(\mathbf{r}) - v_{xc}^-(\mathbf{r})$, cannot be described when the exchange-correlation (xc) potential explicitly (and smoothly) depends only on the density and its derivative. In LDA/GGA, $v_{xc}^{LDA/GGA}(\mathbf{r}) \sim (v_{xc}^+(\mathbf{r}) + v_{xc}^-(\mathbf{r}))/2$, implying roughly that $\epsilon_{HOMO}^{LDA/GGA} = -IP + \Delta_{xc}/2$, and $\epsilon_{LUMO}^{LDA/GGA} = -EA - \Delta_{xc}/2$. As a result, CT excitation energies are underestimated by $\frac{1}{2}(\Delta_{xc}^A + \Delta_{xc}^D)$.[27] This underestimation has been rationalized from a different perspective,[18] and a particularly stark numerical example can be found in Ref 32.

In exact KS theory, the asymptotic potential can be chosen such that $\epsilon_{HOMO} = -IP$, which can be seen by analyzing how the density decays from the perspectives of the interacting and KS systems.[33,34] To be precise, Perdew et al. proved[29,35] that for $Z - 1 < N < Z$ and thus as N approaches Z from below, ϵ_{HOMO} is equal to the negative of the vertical IP of the $N = Z$ electron system. Analogously, it was shown that for $Z < N < Z + 1$, ϵ_{HOMO} of the $N = Z + \delta$ system ($0 < \delta < 1$) equals the negative of the vertical EA of the $N = Z$ electron system. However, taking the limit from below, to ensure that $\epsilon_{HOMO} = -IP$, one finds that $\epsilon_{LUMO} = -EA - \Delta_{xc}$, where the derivative discontinuity can be sizable (in some cases, several eV[34,36]). Evidently, within the KS framework both equalities in Eq. 1 cannot simultaneously be satisfied.

They can, in principle, within the framework of Generalized (G) KS theory,[37] which refers to an exact mapping onto a single-particle system with an effective potential that need not be local. This typically involves the incorporation of a fraction (for global hybrid functionals) or the long-range part (for range-separated hybrid functionals) of the orbital-dependent, non-local exact exchange operator, which leaves a local, "remainder" potential that differs from that in the KS mapping. As non-local exchange has the requisite flexibility to more effectively

reproduce the derivative discontinuity, the amount that has to be reproduced by the local remainder potential in GKS can be reduced more or less systematically. This strategy offers a promising route toward the mitigation of delocalization error and the realization of Eq. 1. As will be shown in this work, CT excitation energies computed within TDDFT using global hybrid functionals are still underestimated (though less so compared to when pure functionals are used), in part because only a small fraction (e.g. 20 and 25% for B3LYP and PBE0, respectively) of the exact exchange is incorporated. Range-separated hybrid (RSH) functionals[38–40] split the electron-electron interaction into short- and long-range parts with respect to a predetermined distance specified by the parameter ω, and treat the latter with the full orbital-dependent exchange operator. RSH functionals provide the flexibility which can allow for, but not guarantee, the desired physical interpretation of the HOMO and LUMO eigenvalues that would make CT excitation energies from TDDFT exact in the infinitely-separated limit. In fact, these functionals, by construction, recover the asymptotically correct $1/R$ long-range behavior, and thus exact CT values in the more relevant Mulliken limit,[41] characterized by well-separated D and A orbitals that do not overlap but nevertheless permit a Coulomb attraction between the transferred electron and hole, are also attainable. We refer readers to Ref. 34 which shows this explicitly.

However, considering that when $\omega \to 0$ the RSH is equivalent to a pure functional (with convex curvature in E vs N), and that when $\omega \to \infty$ the entire range of the electron-electron interaction is treated with HF exchange (which is likely to yield concave curvature as in HF theory), the optimal choice of ω warrants close attention. Furthermore, it has been shown to be challenging for a fixed value of ω to consistently produce accurate results across a range of molecular sizes and excited state characters.[42,43] This is, in part, due to the fact that ω is itself a functional of the density[40] and can vary widely depending on the specific system under investigation.[44–46]

A non-empirical, system-dependent procedure[34] for determining an optimal value of ω, which seeks to enforce not only linearity of E vs N but also the correct slopes to the left

and right of $N = Z$, involves minimizing

$$J^2(\omega) = \sum_{N=Z,Z+1} [\epsilon_N^{HOMO}(\omega) - IP_N(\omega)]^2 \qquad (2)$$

As this attempts to ensure that Eq. 1 is satisfied (recall $\epsilon_{LUMO}(N = Z) \approx \epsilon_{HOMO}(N = Z+1)$, and $EA(N = Z) = IP(N = Z+1)$ for vertical excitations calculated at the $N = Z+1$ geometry), such a protocol significantly improves the accuracy of calculated electronic energy gaps,[34,47] and has been shown to minimize delocalization error by approaching the appropriate linear relationship of the energy with respect to fractional particle number.[34,48,49] This "optimal tuning" (OT) procedure has yielded accurate predictions for organic electronic materials,[50] and CT systems such as the low-lying singlet and triplet states of TADF emitters,[51] aromatic D and tetracyanoethylene A systems,[52] conjugated π systems,[46,53–55] and model heterojunctions involving C_{60}.[56,57] In addition, we note a study of the NDI-xThiophene D-A-D system, where adding thiophene units enabled tuning of the optical absorption.[22] The OT approach has also been shown to work well for CT excited states of various coumarin dyes, which have attracted recent attention due to their potential ability to improve the efficiency of dye-sensitized solar cells.[21] OT combined with stochastic orbital approaches has enabled the study of very large systems such as doped Si nanocrystals.[58]

Until very recently,[3,59] most studies benchmarking the accuracy of computational methods for CT excited states consist of a few isolated examples. The available literature specifically for intramolecular CT is scarcer still. This status quo is likely a reflection of the fact that experimental reference values are difficult to obtain. The occupied and virtual orbitals relevant to CT excited states are typically either nearly or exactly orthogonal, which implies nearly or exactly zero-valued oscillator strengths and thus transition intensities. For intermolecular cases, this can occurs when D and A subunits are separated by a large distance; for intramolecular cases with π systems, this can also be caused by a twist angle of ~ 90 degrees which causes the D and A orbital overlap to vanish. Indeed, twisted intramolecular

(TI) CT states, which nevertheless can play critical roles in photorelaxation pathways,[60,61] rarely fluoresce. Yet measurable emission is possible, in general, when there is small but non-zero overlap between D and A orbitals. This can occur, e.g., when the dihedral angle is non-zero but less than 90 degrees, when there is partial mixing of locally excited character, and/or when there exists steric hindrance such that both ground and excited states have a similar twist angle. We note that it is possible for fluorescence to be observed when the TICT excited state can couple to a higher-lying quantum state from which radiative emission is allowed (though in such cases the true TICT excitation energy will be overestimated).

It is also difficult to augment the admittedly small number of available experiments with benchmark-quality computational predictions, as such efforts are infeasible for most relevant systems due to the steep increase in computational cost as a function of system size, as previously discussed. As a result, reliable reference values (e.g. from EOM-CCSDT) can only be obtained for very small systems, and in a small basis set. Finally, an important aspect of this study involves the assessment of implicit solvation models for solvents representing a wide range of polarities. Excitations involving CT states present a notable difficulty in this regard, as reliable predictions demand a balanced treatment of the (typically) non-polar ground-state and excited states with possibly large permanent dipole moments that strongly interact with polar solvents. OT-TDDFT predictions in the gas phase have previously been compared with measurements in methylene chloride solvent via use of a correction term derived from averaged experimental solvatochromic shifts.[52] For truly predictive applications, however, this approach is not possible, and thus it is of considerable interest to investigate the accuracy of implicit solvation models in the context of CT excitations.

In this work, we focus on absorption and emission energies involving TICT excited states. Comprehensive reviews can be found in, e.g., Ref.s 62, 63, and 64. We present an experimental data set of 61 TICT excitations and show that a computational protocol based on TDDFT with OT functionals and employing equilibrium polarizable continuum models (PCM) for solvents of weak polarity (hexanes and toluene) or non-equilibrium PCM for stronger sol-

vents (such as THF and acetonitrile) yields balanced and reasonably accurate results. We investigate the OT-LRC-ωPBE and OT-LRC-ωPBEh (h refers to a hybrid short-range component with 25% exact exchange) density functionals, and compare with the commonly used global hybrid PBE0, and the RSH functionals LRC-ωPBEh and ωB97X-V.

Methods

Data Set Selection

The chemical structures of all molecules are shown in the Supporting Information. From the data set of 27 TADF molecules used in Ref. 65, we selected those emission energies involving a change in dipole moment larger than 4 Debye, as calculated with the OT-LRC-ωPBEh functional. We also searched the literature for reported measurements of TICT absorption or emission, taking Refs. 63 and 62 as starting points. We then did a comprehensive search for TICT emissions in the gas phase, and found appropriate data for 4-(Diisopropylamino)benzonitrile (DIABN) and 3,5-dimethyl-4-(dimethylamino)benzonitrile (MMD). While we are aware of a third TICT emission measured for 1-tert-butyl-6-cyano-1,2,3,4-tetrahydroquinoline (NTC6) in the gas phase, we chose not to include this case due to the reported presence of multiple degenerate yet geometrically distinct CT excited state conformations.[66]

In addition to the 2 gas-phase measurements, our data set is comprised of 5 measurements in either n-hexane or cyclohexane, 32 in toluene (including the 21 TADF molecules), 1 in o-dichlorobenzene, di(n-pentyl) ether, diethyl ether, and dioxane, 3 in DCM, 6 in THF, 6 in acetonitrile, and 2 in DMF. In addition to those discussed above in the TADF set, this full set includes molecules that can roughly be grouped into the following chemical categories: small-molecules such as the well-studied 4-(dimethylamino)benzonitrile (DMABN),[67–71] boron-containing dyads (with phenyl, mesityl, thienyl, trifluoromethyl, pyrrole groups),[72,73] dyads and triads consisting of triply-fused rings (e.g. anthracene, carbazole, acridine)[74–76] or triph-

enyl triazine derivatives.[77]

In searching for measurements to include in this study, we kept in mind that experimental signatures of TICT fluorescence include an observed red-shift and decrease in quantum yield corresponding to an increase in solvent polarity. In addition, the quantum yield of TICT emission is expected to increases with temperature, as rotational conformations become more readily accessible.

We note that all excitations considered were to and from states of singlet spin multiplicity ($S^2 = S_z = 0$).
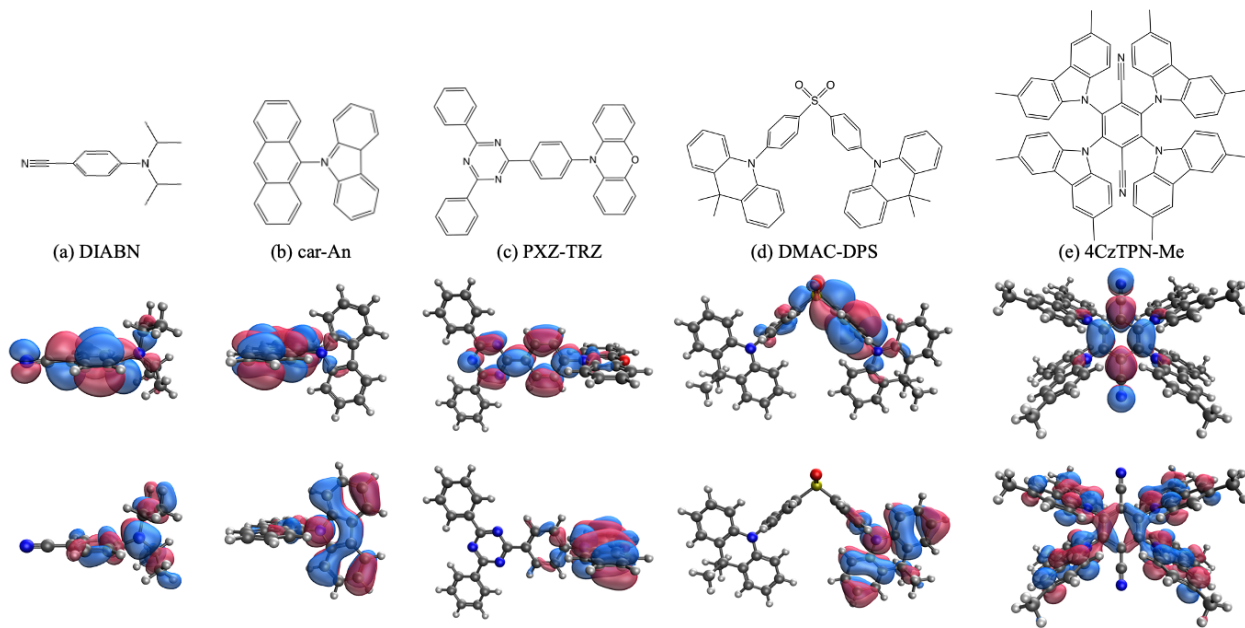

Figure 1: Chemical structures and NTOs of (a) DIABN, (b) car-An, (c) PXZ-TRZ, (d) DMAC-DPS, and (e) 4CzTPN-Me. The dominant donor and acceptor orbitals are displayed in the bottom and middle rows, respectively.

Computational Details

All calculations were performed with Q-Chem 5.2.[78] The def2-SV(P) basis set[79] is used throughout. The geometries of ground (for absorptions) or excited (for emissions) states were optimized with KS DFT or TDDFT, respectively, with the LRC-ωPBEh functional.

OT versions of the LRC-ωPBE and LRC-ωPBEh functionals were obtained by minimizing Eq. 2, in which the IP is obtained from two KS DFT calculations (all computed in the gas phase[80]). The OT functionals were used exclusively in single-point TDDFT calculations.

In this work we consider an excited state to be of significant CT character when either 1) the change in the dipole moment corresponding to a uni-directional electronic transition exceeds 4 Debye, as calculated by the OT-LRC-wPBEh functional, or 2) D and A subunits can be clearly identified from the natural transition orbitals (NTOs) resulting from the LRC-ωPBEh functional used in the geometry optimizations. We note that the target TICT state may *not* be the first excited state at this level of theory.

We utilize PCMs implemented in Q-Chem to approximate the electrostatics of the solute-solvent interactions,[81] as non-electrostatic contributions such as cavitation, dispersion, and Pauli repulsion are typically smaller and more likely to cancel in vertical excitations.[82] The solute cavity surface is discretized with Lebedev spheres via the switching Gaussian (SWIG) method,[83] employing radii determined by Bondi[84] scaled by a factor of 1.2 (or 1.1 for hydrogen[85]). For ground- and excited-state geometry optimizations, and single point TDDFT calculations in hexanes and toluene, the conductor-like PCM is used.[86]

To more accurately model the effects of more polar solvents, we use non-equilibrium approaches, which partition the solvent response into fast (electronic) and slow (nuclear) degrees of freedom, with the IEF-PCM kernel.[81,87] For absorption processes, the solvent field is equilibrated with respect to the solute's electron density in the ground-state, and upon transition to the excited state only the solvent's fast degrees of freedom are allowed to respond.[82,88] Corrections to excitation energies initially computed using solvent-polarized ground-state orbitals are derived from the relaxed density, and contributions are included from both the perturbative linear-response (ptLR) and the perturbative state-specific (ptSS) approaches, since for TDDFT calculations it has been shown that the combination of both yielded better results vs experiment than the use of either one alone.[82] For emission processes, the solvent degrees of freedom are fully relaxed with respect to the CT excited state solute

density via an initial equilibrium PCM calculation. Upon fluorescence, the ground-state is taken to interact with a solvent field which reflects instantaneously adjusted electronic degrees of freedom but nuclear configurations equilibrated with respect to the excited state. This non-equilibrium state-specific calculation is performed self-consistently.[89]

Table 1: Solvent parameters utilized in this work: polarity index (PI), dielectric constant (ϵ), and optical dielectric (ϵ^∞).

	PI	ϵ	ϵ^∞
n-hexane	0.1	1.9	1.89
cyclohexane	0.2	2.0	2.04
toluene	2.4	2.4	2.24
o-dichloro-benzene	2.7	9.9	2.41
di(n-pentyl) ether	2.8†	3.1	1.99
diethyl ether	2.8	4.3	1.83
dichloromethane (DCM)	3.1	8.9	2.03
tetrahydrofuran (THF)	4.0	7.6	1.98
dioxane	4.8	2.3	1.97
acetonitrile	5.8	35.9	1.81
dimethylformamide (DMF)	6.4	36.7	2.05

† In the absence of a literature value, we estimate this to be equal to that of diethyl ether.

All calculations utilize the dielectric constants tabulated in Table 1. Non-equilibrium models require, in addition to the static dielectric constant, the solvent's optical dielectric. This is the dielectric constant at infinite frequency, defined as $\epsilon^\infty = n^2$, where n is the solvent's index of refraction. We note that a solvent's polarity index[90] is not necessarily correlated with its dielectric constant, e.g. dioxane has a smaller dielectric constant but a larger polarity index than toluene.

We ignore vibrational effects throughout, which, along with other finite-temperature effects, effectively puts a lower bound on the accuracy vs experiment that we can expect our computational approach to obtain (we believe this to be at least 0.1 eV).

Results and Discussion

Dependence of the Accuracy on Solvent Strength and Degree of Charge-Transfer

Solvent Strength

In Table 2 we compare calculated results from the equilibrium and non-equilibrium PCM models in five solvents of increasing polarity for the PXZ-TRZ molecule displayed in Figure 1 (c).

Table 2: Experimental emission energies [eV] of PXZ-TRZ in various solvents, and the deviation of calculated values using equilibrium and non-equilibrium PCM.

solvent	expt[a]	ΔOT-LRC-ωPBE/EquilPCM	ΔOT-LRC-ωPBE/nonEquilPCM
n-hexane	2.46	0.00	0.00
toluene	2.28	0.19	0.18
dioxane	2.15	0.31	0.27
o-dichlorobenzene	2.05	0.49	0.26
dichloromethane	1.97	0.57	0.31

[a] Ref. 77

The differences between the equilibrium and non-equilibrium PCM approaches for n-hexane and toluene are 0.00 and 0.01 eV, respectively. As this is well below the level of accuracy we can expect when comparing our calculations to experimental measurements, it will be of little consequence that we utilize equilibrium PCM for these solvents, for simplicity. For the rest of the solvents shown in Table 2, the non-equilibrium PCM is clearly to be preferred (with rather extreme errors of 0.57 eV otherwise obtained). As we are not aware of experimental CT fluoresence data for PXZ-TRZ in very polar solvents such as acetonitrile or DMF, we note that for the emission energy calculated in acetonitrile with the OT-LRC-ωPBEh functional for DIABN and car-An (shown in Figure 1 (a) and (b)), the equilibrium PCM results exceeded those from the non-equilibrium counterpart by 0.34 eV and 0.22 eV, respectively, with predictions from both PCM approaches being above the experimental values.

With a PCM protocol in hand, we proceed to look more carefully at DIABN, as experimental fluorescense measurements are available in the gas phase as well as in a large number of solvents. For each solvent, we calculated the emission energy with a variety of functionals, and the results are shown in Fig. 2.
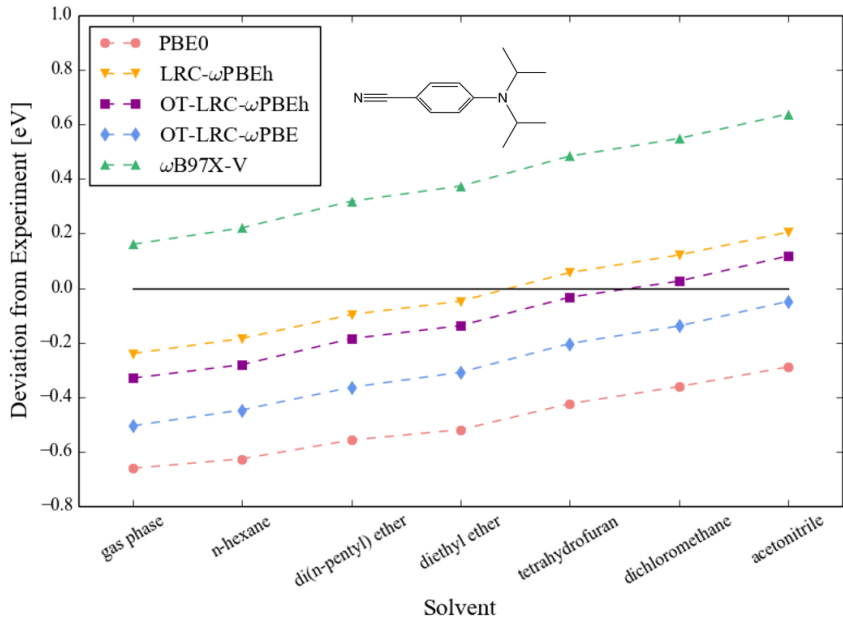

Figure 2: Deviations of the calculated emission energies from experimental values, for the DIABN molecule, in the gas phase and six solvents of increasing polarity. The data points have been connected by dotted lines.

For every solvent, PBE0 and OT-LRC-ωPBE underestimate while ωB97X-V overestimates the measured values. Yet perhaps the most striking observation is that the dependence on solvent strength, among all functionals examined, is nearly uniform (as implied by the connecting lines having nearly identical slopes). This is more clearly revealed in Fig. 3, in which the deviation is plotted not from experiment but from the gas-phase value within a given functional. The near insensitivity (to DFT functional) of the error due to the PCM model is not entirely surprising, since the charge-density is known to be less sensitive than the energy to the functional employed. However, global hybrid functionals in general exhibit a larger degree of delocalization error than RSH variants, which may explain the slight but notable discrepancy for PBE0 compared to the other functionals in Fig. 3.
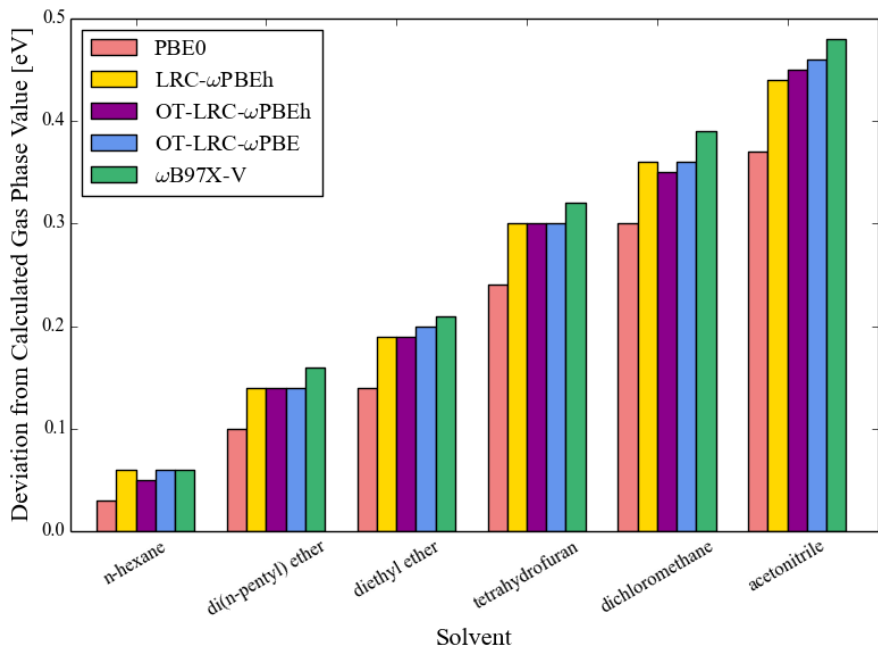
Figure 3: Deviations [eV] of the calculated emission energies for DIABN in a range of solvents from that calculated in the gas-phase with respect to the same density functional.

Magnitude of the Change in Dipole Moment

Another factor in addition to the nature of the solvent, which we have found to significantly affect the accuracy of predicted excitation energies to TICT states, is the degree of CT. To see this, we have controlled for the effect of solvent polarity by selecting all measurements in our data set that were made in toluene solvent. In addition, we have removed CT excitations which involve CT that can be observed in the NTO plots, but which are not reflected in the change in dipole moment due to symmetry. 4CzTPN-Me is an example of this situation, which can be seen in Fig. 1 (e). The transitions shown in Fig. 1 (a)-(d), in contrast, are uni-directional, and thus the degree of CT can be quantified (by a single number in a visualization-free way) by the change in dipole moment. In Fig. 4 we plot the deviations of predictions from the PBE0, LRC-ωPBEh, and OT-LRC-ωPBEh functionals from experiment as a function of the change in dipole moment (in the range 7-21 Debye) for the 24 relevant data points, and show the trendlines parameterized by least-squares fitting.
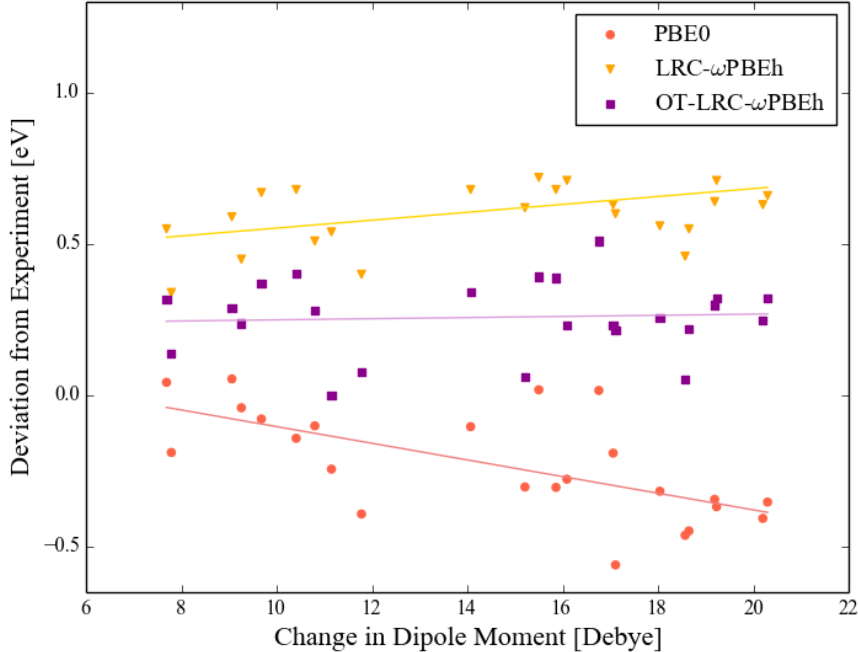
Figure 4: Deviations [eV] from experiment for all measurements in toluene solvent involving changes in dipole moments in the range of 7 and 21 Debye. The slopes of the least-squares regression lines are -0.03, 0.01, and 0.00 for PBE0, LRC-ωPBEh, and OT-LRC-ωPBEh. R^2 values are 0.42, 0.14, and 0.00, respectively.

The calculated values resulting from the PBE0 functional are, unsurprisingly, mostly below the experimental measurements, and notably become more negative as the change in dipole moment increases. Introduction of the range-correction scheme, as represented by the LRC-ωPBEh functional, overcorrects for the underestimation, putting the excitation energies $\sim$0.5 eV above the experimental results. Interestingly, the linear fit of the data-points resulting from the OT hybrid functional has a slope and R^2 of 0.00, implying that the accuracy of its predictions is, on average, independent of the magnitude of the change in dipole moment.

TADF Data Set

In this section, we test the performance of TDDFT/PCM methods on the subset of candidate TADF emitters presented is Ref 65 that exhibit CT character emissions as specified above.

Representative systems are shown in Fig. 1 (c)-(e), with 21 molecules in total. OT-LRC-ωPBE emerges as the most accurate functional for this set of molecules, with a mean signed error (MSE) half that of PBE0 and OT-LRC-ωPBEh. The maximum error is also 0.12-1.19 eV smaller than those of the other functionals investigated.

Table 3: Mean signed error (MSE), mean absolute error (MAE), and maximum absolute error (MaxAE) for emission energies of the TADF set from Ref. 65, containing 21 molecules. Sorted by MAE.

	MSE	MAE	MaxAE
OT-LRC-ωPBE	0.11	0.18	0.34
PBE0	-0.22	0.24	0.46
OT-LRC-ωPBEh	0.23	0.25	0.51
LRC-ωPBEh	0.62	0.62	1.11
ωB97X-V	1.03	1.03	1.53

We note that the performance of the OT-LRC-ωPBE functional in predicting vertical absorption energies for a set of 17 molecules (most of which are investiged presently) has been studied in Ref. 51, finding an MAE of 0.15 eV. This is comparable and slightly lower than our MAE with respect to vertical emission of 0.18 eV, in line with the fact that emissions are from excited TICT states with substantial charge-separation and fully relaxed with respect to solvent degrees of freedom, placing a heavier burden on the implicit solvation model compared to absorptions from typically non-polar ground-states. In addition, our statistical results for this set are similar to those from Ref. 65, which found for a larger set of 27 TADF emissions (including a small number of cases exhibiting local-excitation character, omitted here) an MSE of -0.44 eV with the PBE0 functional. This may suggest that our geometry optimizations, which utilize the LRC-ωPBEh functional, slightly improve the accuracy of calculated single-point emission energies with the PBE0 functional.

The average difference between fluoresence energies calculated via equilibrium and non-equilibrium PCM is 0.02 eV, with a maximum of 0.03 eV. As the latter falls well below our expected level of resolution in comparing with experiments (discussed above), the data in Table 3 reflects the use of equilibrium PCM.

18

Full Data Set

In this section, we consider all 61 absorption and emission measurements involving TICT excited states. All structures, calculated excitation energies, and optimized ω values are presented in the Supporting Information.

Table 4: Mean signed error (MSE), mean absolute error (MAE), and maximum absolute error (MaxAE) for the full set of 61 excitation energies involving TICT excited states included in this study.

	MSE	MAE	MaxAE
OT-LRC-ωPBE	0.02	0.18	0.50
OT-LRC-ωPBEh	0.15	0.21	0.51
PBE0	-0.30	0.30	0.68
LRC-ωPBEh	0.44	0.47	1.11
ωB97X-V	0.83	0.83	1.53

A statistical representation of the accuracy from the five functionals investigated is shown in Table 4. While, as before, the systematic underestimation of the PBE0 functional (MSE of -0.3 eV) and overestimation of the LRC-ωPBEh and ωB97X-V functionals (MSEs of 0.4 and 0.8 eV) are readily apparent, the exceptionally balanced performance of the OT-LRC-ωPBE functional is reflected in its MSE of 0.02 eV. The MAE of 0.18 eV also compares favorably against the other functionals, only slightly lower than that of OT-LRC-ωPBEh but more significantly so when compared with those of the others.

The maximum signed error of OT-LRC-ωPBE, at -0.50 eV corresponding to the gas-phase emission of DIABN, is admittedly undesirable. Yet it is interesting to observe that the second and third largest errors (also underestimations) arise from the emissions of the same molecule in n-hexane and MMD in the gas-phase, respectively. The optimized values of ω are 0.241 and 0.242 for DIABN in the gas-phase and n-hexane, respectively, and 0.261 for MMD. These are quite close to the value of 0.3 that defines the un-tuned LRC-ωPBE functional. Similarly, for OT-LRC-ωPBEh the optimized values of ω for these three cases are 0.180, 0.179, and 0.198 compared with the value of 0.2 that defines the un-tuned LRC-ωPBEh functional. This suggests that the OT procedure results in a minimal modification of

the degree of delocalization error originally present in the parent LRC-ωPBE/h functionals.

This is likely due to the relatively small size of these molecules (DIABN and MMD are, in fact, two of the smallest D-A molecules in the entire set), as it may be the case that the degree of overlap between D and A orbitals is greater (indeed, see Fig. 1 (a)) compared to that in larger molecules which can accommodate stricter orthogonality. In fact, while the other two small molecules, DMABN and n-phenyl pyrrole (PP), only exhibit measurable TICT emissions in strongly polar solvents such as acetonitrile, the trend shown in Fig. 2 would imply that calculated gas-phase values would also severely underestimate experimental measurements (if they were possible). While further investigation is required to draw definitive conclusions, it is reasonable to suppose that for small molecules the underestimation vs experiments in the gas phase and weak solvents may be due to phenomena that are distinct from delocalization error, e.g. correlation effects that are magnified by a small D-A separation. As discussed in the Introduction, a physically rigorous theory of single-electron CT excitations must include not only the D-A transition, but also the instantaneous rearrangements of the electrons in close proximity to the hole on the D subunit and separately to the new charge residing on the A subunit. The degree of required rearrangement may well be reduced by screening effects if the D and A subunits are both sufficiently large, and in such cases TDDFT methods, which can only directly describe single excitations without relaxation effects, can produce accurate CT excitation energies. However, the small D and A subunits found in DMABN, DIABN, MMD, and PP may lead to strong, un-screened electrostatics that require significant, *correlated* charge rearrangements for more than 1 electron. While CC theories including triple excitations are costly to perform (especially in the CBS limit, as would be required to compare with DFT predictions), empirical insight can be gleaned from ΔSCF approaches, in which an excited state is computed variationally such that the orbitals are optimized in the presence of a target excitation. In the particular case of CT, the ROKS method can be utilized to target a singly excited state, and the orbitals can be relaxed to accommodate the presence of the hole and electron on the D and A subunits,

respectively. Results for the two small molecules, DIABN and MMD in the gas-phase, and two representative larger molecules, carBFMes$_2$ and PXZ-TRZ in cyclohexane, are shown in Table 5. With the OT-LRC-ωPBE functional, the ROKS approach reduces the deviation from experiments by $\sim$0.3 eV for the small molecules. This is indirect evidence that relaxation effects (perhaps more so than the mitigation of delocalization error) are critical for an accurate description of CT states in these two cases. For the two larger molecules, TDDFT and ROKS with the OT-LRC-ωPBE functional produce very similar results, suggesting that relaxation effects are relatively less important in these cases. Finally, we note that while the ωB97X-V functional is clearly not optimal for the present TDDFT calculations, very high accuracy is obtained within the ROKS approach for the small molecules, which may be due to its extensive parameterization for variational calculations on similar molecules and the inclusion of VV10 nonlocal correlation.[91] The large sizes of carBFMes$_2$ and PXZ-TRZ are likely not well-represented in the training set employed, and thus the errors from ωB97X-V are not unexpected given the known sensitivity of ω.
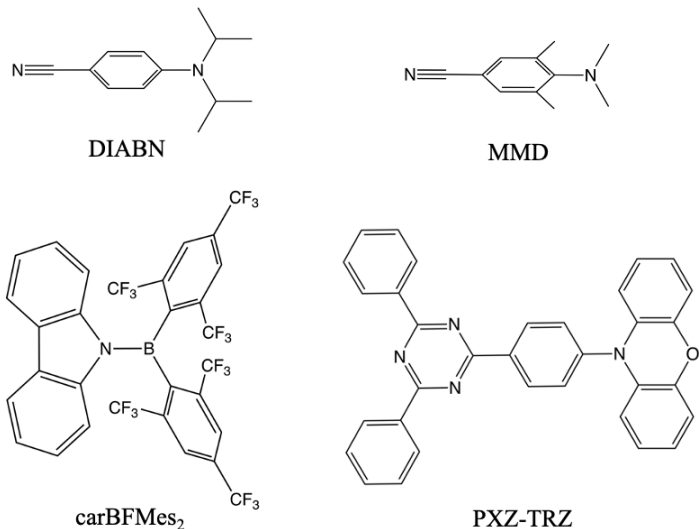

Figure 5: Chemical structures relevant to Table 5.

We mention here, for completeness, two other factors which may play a part in explaining the drastic underestimations in the small molecules within the OT-TDDFT aproach. With overlapping D-A orbitals, the coupling of TICT states to fluorescent excited states of higher

Table 5: Comparison of the experimental and calculated emission energies of representative small (DIABN, MMD) and large (CarBFMes$_2$, PXZ-TRZ) molecules, computed with TDDFT and ROKS methodologies. For the smaller molecules in the top-half of the table, all values correspond to the gas-phase. For the larger molecules in the bottom-half, experimental measurements were taken in cyclohexane solvent; the TD/OT-LRC-ωPBE calculations utilized equilibrium PCM, while the ROKS calculations were performed in the gas-phase and corrected[†] to reflect cyclohexane solvent.

	expt	ΔTD/OT-LRC-ωPBE	ΔROKS/OT-LRC-ωPBE	ΔROKS/ωB97X-V
DIABN	3.26	-0.50	-0.19	0.03
MMD	3.22	-0.41	-0.10	0.09
CarBFMes$_2$	2.06	-0.04	-0.06[†]	0.32[†]
PXZ-TRZ	2.45	0.00	0.16[†]	0.51[†]

[†] Obtained by correcting the value calculated in the gas-phase by the energy difference between the OT-LRC-ωPBE results in cyclohexane and the gas-phase.

energy may be enhanced,[63] which could explain the discrepancy between our calculations and experiment by claiming that the latter is an overestimate of the targeted TICT state's excitation energy. Alternatively, the large deviations could be due to the use of incorrect geometries in our calculation, which is not unlikely in light of the presence of conflicting claims in the literature, e.g. an X-ray crystal structure which suggests the CT state of DIABN has a dihedral angle of only 10 degrees,[92] and a computational study using CC-based methods which finds not only a 90 degree dihedral but a distortion from C$_{2v}$ symmetry to C_s corresponding to pyramidalization of the carbon adjacent to the amino group[93] (in agreement with the one used here, shown in Fig. 1 (a)). It is also possible that for DIABN or MMD there could be multiple degenerate CT excited states of distinct conformations and emission energies, as was found for NTC6 in the gas phase.[66] In any case, it is revealing to note that if DIABN and MMD are omitted from the test set, the MaxAE would be substantially reduced to 0.34 eV (for PIC-TRZ).

Another observation which strengthens the hypothesis that effects other than delocalization error are responsible for the largest deviations from experiment for small molecules, is that the MSEs for subsets of the 61 molecules, grouped by solvent strength, do not show the expected trends. As shown on the right-side of Table 6, the MSEs from the OT-LRC-ωPBE functional do not consistently increase as the solvent polarity increases, for PI > 2.4.

However, when the measurements associated with the four small DMABN-like molecules are excluded, along with the single cationic species (MesArc$^+$), the expected trends are indeed recovered in the relative MSEs. To be specific, we binned solvents by polarity index into four categories: 1) hexanes (PI = 0.1-0.2), 2) toluene (PI = 2.4), 3) o-dichlorobenzene, di(n-pentyl) ether, diethyl ether, DCM, THF, dioxane (PI = 2.7-4.8), and 4) acetonitrile, DMF (PI = 5.8-6.4). The left-side of Table 6 reveals that the MSEs indeed increase with solvent strength across all four groups, and a reduced maximum error (from 0.50 to 0.34 eV) is obtained.

Table 6: Mean signed error (MSE), mean absolute error (MAE), and maximum absolute error (MaxAE) for the OT-LRC-ωPBE functional, for the dataset sorted by solvent polarity index (PI).

PI	MSE†	MAE†	MaxAE†	MSE	MAE	MaxAE
0 (gas)				-0.46	0.46	0.50
0.1-0.2	-0.04	0.04	0.07	-0.12	0.12	0.45
2.4	0.07	0.16	0.34	0.07	0.16	0.34
2.7-4.8	0.11	0.19	0.31	0.00	0.21	0.36
5.8-6.4	0.17	0.18	0.25	0.08	0.16	0.25
All	0.08	0.16	0.34	0.02	0.18	0.50

† With measurements corresponding to 4 small molecules (DMABN, DIABN, MMD, PP) and charged species (Mes-Acr$^+$) removed.

One may wonder how a theory constrained to the space of single-excitations, such as TDDFT within the adiabatic approximation, can so accurately describe CT excitations at all! From the wavefunction perspective, one would expect that two-body excitation operators at a minimum are required to account for relaxation in the presence of the new hole or charge, and that three-body operators would be needed to rigorously account for the D to A excitation plus the relaxation of both the D and A subunits (as previously discussed). The picture that our data paints is that while linear combinations of single-excitations are insufficient to adequately describe TICT excitation energies for small D-A molecules, the level of theory is, on average, adequate for medium to large-sized molecules. This empirical finding is, rather beautifully, consistent with what should be expected from analyzing the exactness of the TDDFT equations in the well-separated D and A limit, namely that OT-TDDFT

with RSH functionals is indeed rigorously optimal only in this limit, and should therefore not be expected to improve CT excitation energies when D and A units significantly overlap. Fortunately, in most applications, the larger system sizes are more relevant than small ones, though methods such as ROKS appear to be a promising alternative to OT-TDDFT for the latter.

Conclusions and Outlook

In this work, the accuracy of TDDFT/PCM to describe TICT excitation energies in solution has been explored. For a fixed molecule in various solvents, we reveal a systematic tendency, that is manifest in all functionals investigated, for the deviation between calculated CT excitation energies and experimental measurements to become more positive (but not necessarily larger in magnitude) with solvent polarity, due to the increasing inability of the employed non-equilibrium PCM method to fully account for the stabilization effects which increase in magnitude with the polarity of the solvent. Secondly, we show evidence that non-empirical tuning of RSH functionals removes the dependence of the accuracy on the degree of CT, as quantified by the change in dipole moment during the electronic transition. In a fixed solvent, we find the deviations from experiment are approximately constant for a range of dipole moment changes between 7 and 21 Debye. We find encouraging statistical accuracy from the OT-LRC-ωPBE functional for a set of 21 medium to large-sized molecules relevant to TADF in toluene solvent. For the full data set of 61 measurements in the gas phase and solvents ranging from hexanes to acetonitrile, we find an MSE and MAE of 0.02 and 0.18 eV. Removing the measurements taken for the four small molecules, along with the only cation considered, reveals the expected trend, i.e. when grouped according to polarity index, MSEs increase in tandem with the solvent strength. This, in addition to a decrease in maximum error from 0.50 to 0.34 eV, and the small deviation found between optimized and original values of the ω parameter for the small molecules, also lends evidence to the hypothesis that

the large errors encountered only for small molecules are *not* a result of delocalization error, but reflect a larger degree of electron relaxation effects (perhaps due to reduced screening) in response to the one-electron CT excitation when D and A subunits are small. The improved accuracy of ROKS calculations with the same OT functional utilized in TDDFT, which allow for orbital relaxation in variationally optimized excited states, for these cases lends further support and indeed implicates the limitation to the subspace of single-excitations as the source of the large deviations that result from (even OT) adiabatic TDDFT in the case of small molecules. This is consistent with the fact that the OT procedure can only be expected to yield exact TDDFT results in the Mulliken limit (and beyond), and may not be useful when shorter D-A distances enable non-negligible orbital overlap.

Many of the main conclusions of this work can be summarized and illustrated with the (1,4)-phenylene-linked zincbacteriochlorinbacteriochlorin complex (ZnBC-BC), a biomimetic model system for light-harvesting complexes in Photosystem II, drawn in Fig. 6. This dyad exhibits CT excited states with dipole moments of ~60 Debye (as calculated by OT-LRC-ωPBEh), and Table 7 presents gas-phase absorption energies from various computational methods.
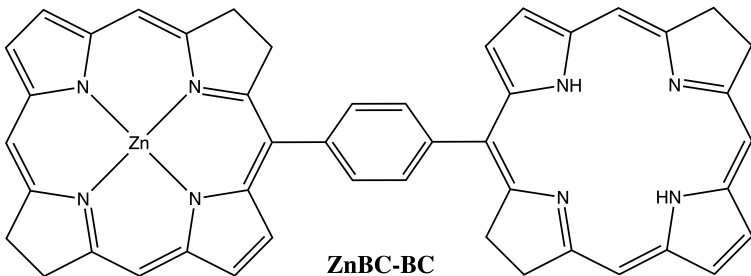

Figure 6: Chemical structure of ZnBC-BC.

Compared to GW/BSE predictions,[95] PBE0 underestimates by an entire eV, consistent with similarly large failures noted in Ref.s 32, 96, and 97 along with those shown herein, while commonly used RSH functionals overestimate by roughly half an eV or more. The OT functionals both show reduced errors from that resulting from the LRC-ωPBEh functional, and compare reasonably with predictions from GW/BSE (as found previously for

Table 7: Calculated excitation energies [eV] corresponding to CT absorptions of ZnBC-BC in the gas phase.

	LRC-ωPBEh	OT-LRC-ωPBEh[†]	OT-LRC-ωPBE[††]	PBE0	ωB97X-V	CAM-B3LYP[a]	GW/BSE[b]
ZnBC→BC	3.44	3.14	3.20	1.99	3.70	2.87	2.95
ZnBC←BC	3.60	3.30	3.34	2.17	3.86	3.04	3.13

[a] Ref. 94. 6-31G* basis set.
[b] Ref. 95
[†] $\omega = 0.141$
[††] $\omega = 0.180$

intermolecular CT systems[98]) and CAM-B3LYP.[94]

While this work demonstrates that OT-LRC-ωPBE/h functionals can accurately describe TICT excitations of large molecules within the TDDFT framework, we mention a number of current limitations that warrant future research. Chief among these is the lack of size-consistency due to the OT, making thermochemical predictions of, e.g., reaction profiles precarious. The fact that different ω values reflect the use of different functionals, more generally, prevents rigorous comparisons of energetic quantities derived from different molecular geometries. We note signs of progress in this direction,[45] though we do so with somewhat muted expectations as the known (formally and empirically) dependence of ω on the density (and thus indirectly on the geometry/system-size) would suggest that a single ω cannot be simultaneously optimal for all species involved in, e.g., the calculation of an atomization energy. Also, while the OT procedure appears to effectively mitigate errors that result from delocalization error, predicted excitation energies from adiabatic TDDFT will still be unpredictable and large in the case of double (or higher particle number) excitations,[99] and in the presence of substantial static electron correlation in the ground-state.[100] Errors due to static correlation in the simple model of H_2 can be traced back to unphysical fractional spins in the dissociation limit, and approaches similar in spirit to the OT strategy employed here are being developed.[26] In addition, many instances of ground-state static correlation can be rigorously described within the spin-restricted ensemble-referenced KS (REKS) formalism,[12,101] and its state interaction/averaged extension (SI-SA-REKS) has yielded promising excitation energies for arene-tetracyanoethylene CT states.[102] For practical applications of the OT-TDDFT method studied here, we recommend first checking if the predicted local

excitation agrees with, e.g., an experimental absorption spectrum. If so, the OT protocol described herein is likely to yield good accuracy for associated CT states. Finally we note that the PCM, including non-equilibrium variants, also has well-known limitations such as the inability to describe hydrogen bonding effects, which are nevertheless critical in many areas of biology. Future work will involve more comprehensively exploring other PCMs for electrostatics,[103] and also the inclusion of non-electrostatic solvent-solute interaction terms.[104]

As more experimental TICT absorption and fluoresence measurements (and/or benchmark-quality *ab initio* predictions) become available, we envision the possibility of proposing empirical corrections to OT functionals, e.g., based on the solvent, or preferably more direct functional development. The present data set, while certainly not yet as large or diverse as we would like, has enabled us to glean valuable insights about the promising performance of OT RSH density functionals together with implicit solvation models.
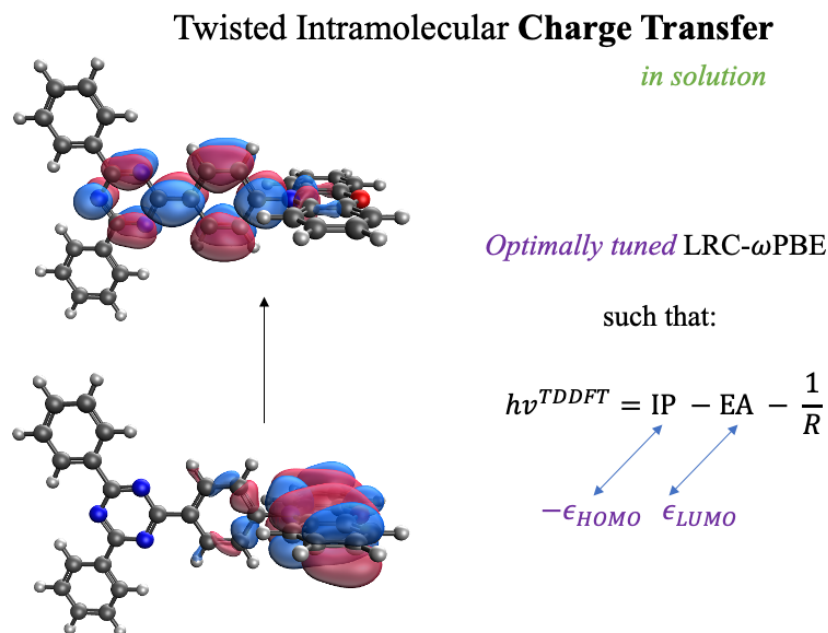

Figure 7: Table of Contents Figure

Acknowledgement

Supporting Information Available

The Supporting Information is available free of charge on the ACS Publications website at DOI:

Chemical structures, tabulated excitation energies and optimal values of ω, Cartesian coordinates

References

(1) Friend, R.; Gymer, R.; Holmes, A.; Burroughes, J.; Marks, R.; Taliani, C.; Bradley, D.; Dos Santos, D.; Bredas, J.; Lögdlund, M., et al. Electroluminescence in conjugated polymers. *Nature* **1999**, *397*, 121–128.

(2) Uoyama, H.; Goushi, K.; Shizu, K.; Nomura, H.; Adachi, C. Highly efficient organic light-emitting diodes from delayed fluorescence. *Nature* **2012**, *492*, 234–238.

(3) Kozma, B.; Tajti, A.; Demoulin, B.; Izsák, R.; Nooijen, M.; Szalay, P. G. A New Benchmark Set for Excitation Energy of Charge Transfer States: Systematic Investigation of Coupled-Cluster Type Methods. *J. Chem. Theory Comput.* **2020**,

(4) Nooijen, M.; Bartlett, R. J. Similarity transformed equation-of-motion coupled-cluster theory: Details, examples, and comparisons. *J. Chem. Phys.* **1997**, *107*, 6812–6830.

(5) Dutta, A. K.; Nooijen, M.; Neese, F.; Izsak, R. Exploring the accuracy of a low scaling

similarity transformed equation of motion method for vertical excitation energies. *J. Chem. Theory Comput.* **2018**, *14*, 72–91.

(6) Schreiber, M.; Silva-Junior, M. R.; Sauer, S. P.; Thiel, W. Benchmarks for electronically excited states: CASPT2, CC2, CCSD, and CC3. *J. Chem. Phys.* **2008**, *128*, 134110.

(7) Berraud-Pache, R.; Neese, F.; Bistoni, G.; Izsák, R. Unveiling the photophysical properties of Boron-dipyrromethene dyes using a new accurate excited state coupled cluster method. *J. Chem. Theory Comput.* **2019**,

(8) Loos, P.-F.; Scemama, A.; Blondel, A.; Garniron, Y.; Caffarel, M.; Jacquemin, D. A mountaineering strategy to excited states: Highly accurate reference energies and benchmarks. *J. Chem. Theory Comput.* **2018**, *14*, 4360–4379.

(9) Hoyer, C. E.; Gagliardi, L.; Truhlar, D. G. Multiconfiguration pair-density functional theory spectral calculations are stable to adding diffuse basis functions. *J. Phys. Chem. Lett.* **2015**, *6*, 4184–4188.

(10) Ziegler, T.; Rauk, A.; Baerends, E. J. On the calculation of multiplet energies by the Hartree-Fock-Slater method. *Theor. Chim. Acta* **1977**, *43*, 261–271.

(11) Kowalczyk, T.; Yost, S. R.; Voorhis, T. V. Assessment of the ΔSCF density functional theory approach for electronic excitations in organic dyes. *J. Chem. Phys.* **2011**, *134*, 054128.

(12) Filatov, M.; Shaik, S. Spin-restricted density functional approach to the open-shell problem. *Chem. Phys. Lett.* **1998**, *288*, 689–697.

(13) Kowalczyk, T.; Tsuchimochi, T.; Chen, P.-T.; Top, L.; Van Voorhis, T. Excitation energies and Stokes shifts from a restricted open-shell Kohn-Sham approach. *J. Chem. Phys.* **2013**, *138*, 164101.

(14) Hait, D.; Head-Gordon, M. Excited State Orbital Optimization via Minimizing the Square of the Gradient: General Approach and Application to Singly and Doubly Excited States via Density Functional Theory. *J. Chem. Theory Comput.* **0**, *0*, null, PMID: 32017554.

(15) Gaudoin, R.; Burke, K. Lack of Hohenberg-Kohn theorem for excited states. *Phys. Rev. Lett.* **2004**, *93*, 173001.

(16) Runge, E.; Gross, E. K. Density-functional theory for time-dependent systems. *Phys. Rev. Lett.* **1984**, *52*, 997.

(17) Casida, M. E. *Recent Advances In Density Functional Methods: (Part I)*; World Scientific, 1995; pp 155–192.

(18) Dreuw, A.; Head-Gordon, M. Single-reference ab initio methods for the calculation of excited states of large molecules. *Chem. Rev.* **2005**, *105*, 4009–4037.

(19) Rohrdanz, M. A.; Herbert, J. M. Simultaneous benchmarking of ground-and excited-state properties with long-range-corrected density functional theory. *J. Chem. Phys.* **2008**, *129*, 034107.

(20) Rohrdanz, M. A.; Martins, K. M.; Herbert, J. M. A long-range-corrected density functional that performs well for both ground-state properties and time-dependent density functional theory excitation energies, including charge-transfer excited states. *J. Chem. Phys.* **2009**, *130*, 054112.

(21) Stein, T.; Kronik, L.; Baer, R. Prediction of charge-transfer excitations in coumarin-based dyes using a range-separated functional tuned from first principles. *J. Chem. Phys.* **2009**, *131*, 244119.

(22) Karolewski, A.; Stein, T.; Baer, R.; Kümmel, S. Communication: Tailoring the optical gap in light-harvesting molecules. *J. Chem. Phys.* **2011**, *134*, 151101.

(23) Gross, E.; Dobson, J.; Petersilka, M. *Density functional theory II*; Springer, 1996; pp 81–172.

(24) Burke, K.; Werschnik, J.; Gross, E. Time-dependent density functional theory: Past, present, and future. *J. Chem. Phys.* **2005**, *123*, 062206.

(25) Mori-Sánchez, P.; Cohen, A. J.; Yang, W. Many-electron self-interaction error in approximate density functionals. *J. Chem. Phys.* **2006**, *125*, 201102.

(26) Cohen, A. J.; Mori-Sánchez, P.; Yang, W. Insights into current limitations of density functional theory. *Science* **2008**, *321*, 792–794.

(27) Tozer, D. J. Relationship between long-range charge-transfer excitation energy error and integer discontinuity in Kohn–Sham theory. *J. Chem. Phys.* **2003**, *119*, 12697–12699.

(28) Cohen, A. J.; Mori-Sánchez, P.; Yang, W. Challenges for density functional theory. *Chem. Rev.* **2012**, *112*, 289–320.

(29) Perdew, J. P.; Parr, R. G.; Levy, M.; Balduz Jr, J. L. Density-functional theory for fractional particle number: derivative discontinuities of the energy. *Phys. Rev. Lett.* **1982**, *49*, 1691.

(30) Yang, W.; Zhang, Y.; Ayers, P. W. Degenerate ground states and a fractional number of electrons in density and reduced density matrix functional theory. *Phys. Rev. Lett.* **2000**, *84*, 5172.

(31) Szabo, A.; Ostlund, N. S. *Modern quantum chemistry: introduction to advanced electronic structure theory*; Courier Corporation, 2012.

(32) Dreuw, A.; Head-Gordon, M. Failure of time-dependent density functional theory for long-range charge-transfer excited states: the zincbacteriochlorin- bacteriochlorin and bacteriochlorophyll- spheroidene complexes. *J. Am. Chem. Soc.* **2004**, *126*, 4007–4016.

(33) Almbladh, C.-O.; von Barth, U. Exact results for the charge and spin densities, exchange-correlation potentials, and density-functional eigenvalues. *Phys. Rev. B* **1985**, *31*, 3231.

(34) Kronik, L.; Stein, T.; Refaely-Abramson, S.; Baer, R. Excitation gaps of finite-sized systems from optimally tuned range-separated hybrid functionals. *J. Chem. Theory Comput.* **2012**, *8*, 1515–1531.

(35) Perdew, J. P.; Levy, M. Comment on "Significance of the highest occupied Kohn-Sham eigenvalue". *Phys. Rev. B* **1997**, *56*, 16021.

(36) Allen, M. J.; Tozer, D. J. Eigenvalues, integer discontinuities and NMR shielding constants in Kohn—Sham theory. *Mol. Phys.* **2002**, *100*, 433–439.

(37) Seidl, A.; Görling, A.; Vogl, P.; Majewski, J. A.; Levy, M. Generalized Kohn-Sham schemes and the band-gap problem. *Phys. Rev. B* **1996**, *53*, 3764.

(38) Tawada, Y.; Tsuneda, T.; Yanagisawa, S.; Yanai, T.; Hirao, K. A long-range-corrected time-dependent density functional theory. *J. Chem. Phys.* **2004**, *120*, 8425–8433.

(39) Iikura, H.; Tsuneda, T.; Yanai, T.; Hirao, K. A long-range correction scheme for generalized-gradient-approximation exchange functionals. *J. Chem. Phys.* **2001**, *115*, 3540–3544.

(40) Baer, R.; Neuhauser, D. Density functional theory with correct long-range asymptotic behavior. *Phys. Rev. Lett.* **2005**, *94*, 043002.

(41) Mulliken, R. S. Molecular compounds and their spectra. II. *J. Am. Chem. Soc.* **1952**, *74*, 811–824.

(42) Peach, M. J.; Cohen, A. J.; Tozer, D. J. Influence of Coulomb-attenuation on exchange–correlation functional quality. *Phys. Chem. Chem. Phys.* **2006**, *8*, 4543–4549.

(43) Huang, S.; Zhang, Q.; Shiota, Y.; Nakagawa, T.; Kuwabara, K.; Yoshizawa, K.; Adachi, C. Computational prediction for singlet-and triplet-transition energies of charge-transfer compounds. *J. Chem. Theory Comput.* **2013**, *9*, 3872–3877.

(44) Livshits, E.; Baer, R. A well-tempered density functional theory of electrons in molecules. *Phys. Chem. Chem. Phys.* **2007**, *9*, 2932–2941.

(45) Livshits, E.; Baer, R. A density functional theory for symmetric radical cations from bonding to dissociation. *J. Phys. Chem. A* **2008**, *112*, 12789–12791.

(46) Körzdörfer, T.; Sears, J. S.; Sutton, C.; Brédas, J.-L. Long-range corrected hybrid functionals for π-conjugated systems: Dependence of the range-separation parameter on conjugation length. *J. Chem. Phys.* **2011**, *135*, 204107.

(47) Stein, T.; Eisenberg, H.; Kronik, L.; Baer, R. Fundamental gaps in finite systems from eigenvalues of a generalized Kohn-Sham method. *Phys. Rev. Lett.* **2010**, *105*, 266802.

(48) Srebro, M.; Autschbach, J. Tuned range-separated time-dependent density functional theory applied to optical rotation. *J. Chem. Theory Comput.* **2012**, *8*, 245–256.

(49) Srebro, M.; Autschbach, J. Does a molecule-specific density functional give an accurate electron density? The challenging case of the CuCl electric field gradient. *J. Phys. Chem. Lett.* **2012**, *3*, 576–581.

(50) Korzdorfer, T.; Bredas, J.-L. Organic electronic materials: recent advances in the DFT description of the ground and excited states using tuned range-separated hybrid functionals. *Acc. Chem. Res.* **2014**, *47*, 3284–3291.

(51) Sun, H.; Zhong, C.; Bredas, J.-L. Reliable prediction with tuned range-separated functionals of the singlet–triplet gap in organic emitters for thermally activated delayed fluorescence. *J. Chem. Theory Comput.* **2015**, *11*, 3851–3858.

(52) Stein, T.; Kronik, L.; Baer, R. Reliable prediction of charge transfer excitations in molecular complexes using time-dependent density functional theory. *J. Am. Chem. Soc.* **2009**, *131*, 2818–2820.

(53) Sun, H.; Autschbach, J. Influence of the delocalization error and applicability of optimal functional tuning in density functional calculations of nonlinear optical properties of organic donor–acceptor chromophores. *ChemPhysChem* **2013**, *14*, 2450–2461.

(54) Minami, T.; Ito, S.; Nakano, M. Theoretical study of singlet fission in oligorylenes. *J. Phys. Chem. Lett.* **2012**, *3*, 2719–2723.

(55) Kuritz, N.; Stein, T.; Baer, R.; Kronik, L. Charge-transfer-like π π^* excitations in time-dependent density functional theory: A conundrum and its solution. *J. Chem. Theory Comput.* **2011**, *7*, 2408–2415.

(56) Minami, T.; Nakano, M.; Castet, F. Nonempirically tuned Long-Range corrected density functional theory study on local and Charge-Transfer excitation energies in a Pentacene/C60 model complex. *J. Phys. Chem. Lett.* **2011**, *2*, 1725–1730.

(57) Isaacs, E. B.; Sharifzadeh, S.; Ma, B.; Neaton, J. B. Relating trends in first-principles electronic structure and open-circuit voltage in organic photovoltaics. *J. Phys. Chem. Lett.* **2011**, *2*, 2531–2537.

(58) Lee, A. J.; Chen, M.; Li, W.; Neuhauser, D.; Baer, R.; Rabani, E. Dopant levels in large nanocrystals using stochastic optimally tuned range-separated hybrid density functional theory. *arXiv preprint arXiv:2003.01164* **2020**,

(59) Verma, P.; Wang, Y.; Ghosh, S.; He, X.; Truhlar, D. G. Revised M11 exchange-correlation functional for electronic excitation energies and ground-state properties. *J. Phys. Chem. A* **2019**, *123*, 2966–2990.

(60) Ghosh, R.; Palit, D. K. Effect of donor–acceptor coupling on TICT dynamics in the excited states of two dimethylamine substituted chalcones. *J. Phys. Chem. A* **2015**, *119*, 11128–11137.

(61) Wu, E. C.; Ge, Q.; Arsenault, E. A.; Lewis, N. H.; Gruenke, N. L.; Head-Gordon, M. J.; Fleming, G. R. Two-dimensional electronic-vibrational spectroscopic study of conical intersection dynamics: an experimental and electronic structure study. *Phys. Chem. Chem. Phys.* **2019**, *21*, 14153–14163.

(62) Sasaki, S.; Drummen, G. P.; Konishi, G.-i. Recent advances in twisted intramolecular charge transfer (TICT) fluorescence and related phenomena in materials chemistry. *J. Mater. Chem. C* **2016**, *4*, 2731–2743.

(63) Rettig, W. Charge separation in excited states of decoupled systems—TICT compounds and implications regarding the development of new laser dyes and the primary process of vision and photosynthesis. *Angew. Chem., Int. Ed. Engl.* **1986**, *25*, 971–988.

(64) Grabowski, Z. R.; Dobkowski, J. Twisted intramolecular charge transfer (TICT) excited states: energy and molecular structure. *Pure Appl. Chem.* **1983**, *55*, 245–252.

(65) Hait, D.; Zhu, T.; McMahon, D. P.; Van Voorhis, T. Prediction of excited-state energies and singlet–triplet gaps of charge-transfer states using a restricted open-shell Kohn–Sham approach. *J. Chem. Theory Comput.* **2016**, *12*, 3353–3359.

(66) Hättig, C.; Hellweg, A.; Köhn, A. Intramolecular charge-transfer mechanism in quinolidines: The role of the amino twist angle. *J. Am. Chem. Soc.* **2006**, *128*, 15672–15682.

(67) Atsbeha, T.; Mohammed, A. M.; Redi-Abshiro, M. Excitation wavelength dependence of dual fluorescence of DMABN in polar solvents. *J. Fluoresc.* **2010**, *20*, 1241–1248.

(68) Druzhinin, S. I.; Mayer, P.; Stalke, D.; von Bulow, R.; Noltemeyer, M.; Zachariasse, K. A. Intramolecular charge transfer with 1-tert-butyl-6-cyano-1, 2, 3, 4-

tetrahydroquinoline (ntc6) and other aminobenzonitriles. a comparison of experimental vapor phase spectra and crystal structures with calculations. *J. Am. Chem. Soc.* **2010**, *132*, 7730–7744.

(69) Grabowski, Z. R.; Rotkiewicz, K.; Rettig, W. Structural changes accompanying intramolecular electron transfer: focus on twisted intramolecular charge-transfer states and structures. *Chem. Rev.* **2003**, *103*, 3899–4032.

(70) Rotkiewicz, K.; Rubaszewska, W. Intramolecular charge transfer state and unusual fluorescence from an upper excited singlet of a nonplanar derivative of p-cyano-N, N-dimethylaniline. *J. Lumin.* **1982**, *27*, 221–230.

(71) Sarkar, A.; Chakravorti, S. A study on the spectroscopy and photophysics of N-phenyl pyrrole and N-phenyl pyrazole. *Chem. Phys. Lett.* **1995**, *235*, 195–201.

(72) Taniguchi, T.; Wang, J.; Irle, S.; Yamaguchi, S. TICT fluorescence of N-borylated 2, 5-diarylpyrroles: a gear like dual motion in the excited state. *Dalton Trans.* **2013**, *42*, 620–624.

(73) Wang, J.; Wang, Y.; Taniguchi, T.; Yamaguchi, S.; Irle, S. Substituent effects on twisted internal charge transfer excited states of N-borylated carbazoles and (diphenylamino) boranes. *J. Phys. Chem. A* **2012**, *116*, 1151–1158.

(74) Sasaki, S.; Hattori, K.; Igawa, K.; Konishi, G.-i. Directional Control of π-Conjugation Enabled by Distortion of the Donor Plane in Diarylaminoanthracenes: A Photophysical Study. *J. Phys. Chem. A* **2015**, *119*, 4898–4906.

(75) Benniston, A. C.; Harriman, A.; Li, P.; Rostron, J. P.; van Ramesdonk, H. J.; Groeneveld, M. M.; Zhang, H.; Verhoeven, J. W. Charge shift and triplet state formation in the 9-mesityl-10-methylacridinium cation. *J. Am. Chem. Soc.* **2005**, *127*, 16054–16064.

(76) Catalán, J.; Diaz, C.; López, V.; Perez, P.; Claramunt, R. The TICT Mechanism in 9, 9 '-Biaryl Compounds: Solvatochromism of 9, 9 '-Bianthryl, N-(9-Anthryl) carbazole, and N, N '-Bicarbazyl. *J. Phys. Chem.* **1996**, *100*, 18392–18398.

(77) Tanaka, H.; Shizu, K.; Nakanotani, H.; Adachi, C. Twisted intramolecular charge transfer state for long-wavelength thermally activated delayed fluorescence. *Chem. Mater.* **2013**, *25*, 3766–3771.

(78) Shao, Y.; Gan, Z.; Epifanovsky, E.; Gilbert, A. T.; Wormit, M.; Kussmann, J.; Lange, A. W.; Behn, A.; Deng, J.; Feng, X., et al. Advances in molecular quantum chemistry contained in the Q-Chem 4 program package. *Mol. Phys.* **2015**, *113*, 184–215.

(79) Weigend, F.; Ahlrichs, R. Balanced basis sets of split valence, triple zeta valence and quadruple zeta valence quality for H to Rn: Design and assessment of accuracy. *Phys. Chem. Chem. Phys.* **2005**, *7*, 3297–3305.

(80) de Queiroz, T. B.; Kümmel, S. Charge-transfer excitations in low-gap systems under the influence of solvation and conformational disorder: Exploring range-separation tuning. *J. Chem. Phys.* **2014**, *141*, 084303.

(81) Tomasi, J.; Mennucci, B.; Cammi, R. Quantum mechanical continuum solvation models. *Chem. Rev.* **2005**, *105*, 2999–3094.

(82) Mewes, J.-M.; You, Z.-Q.; Wormit, M.; Kriesche, T.; Herbert, J. M.; Dreuw, A. Experimental benchmark data and systematic evaluation of two a posteriori, polarizable-continuum corrections for vertical excitation energies in solution. *J. Phys. Chem. A* **2015**, *119*, 5446–5464.

(83) Lange, A. W.; Herbert, J. M. A smooth, nonsingular, and faithful discretization scheme for polarizable continuum models: The switching/Gaussian approach. *J. Chem. Phys.* **2010**, *133*, 244111.

(84) Bondi, A. v. van der Waals volumes and radii. *J. Phys. Chem.* **1964**, *68*, 441–451.

(85) Rowland, R. S.; Taylor, R. Intermolecular nonbonded contact distances in organic crystal structures: Comparison with distances expected from van der Waals radii. *J. Phys. Chem.* **1996**, *100*, 7384–7391.

(86) Barone, V.; Cossi, M. Quantum calculation of molecular energies and energy gradients in solution by a conductor solvent model. *J. Phys. Chem. A* **1998**, *102*, 1995–2001.

(87) Mennucci, B.; Cances, E.; Tomasi, J. Evaluation of solvent effects in isotropic and anisotropic dielectrics and in ionic solutions with a unified integral equation method: theoretical bases, computational implementation, and numerical applications. *J. Phys. Chem. B* **1997**, *101*, 10506–10517.

(88) You, Z.-Q.; Mewes, J.-M.; Dreuw, A.; Herbert, J. M. Comparison of the Marcus and Pekar partitions in the context of non-equilibrium, polarizable-continuum solvation models. *J. Chem. Phys.* **2015**, *143*, 204104.

(89) Mewes, J.-M.; Herbert, J. M.; Dreuw, A. On the accuracy of the general, state-specific polarizable-continuum model for the description of correlated ground-and excited states in solution. *Phys. Chem. Chem. Phys.* **2017**, *19*, 1644–1654.

(90) Snyder, L. Classification off the Solvent Properties of Common Liquids. *J. Chromatogr. Sci.* **1978**, *16*, 223–234.

(91) Mardirossian, N.; Head-Gordon, M. ωB97X-V: A 10-parameter, range-separated hybrid, generalized gradient approximation density functional with nonlocal correlation, designed by a survival-of-the-fittest strategy. *Phys. Chem. Chem. Phys.* **2014**, *16*, 9904–9924.

(92) Techert, S.; Zachariasse, K. A. Structure determination of the intramolecular charge

transfer state in crystalline 4-(diisopropylamino) benzonitrile from picosecond X-ray diffraction. *J. Am. Chem. Soc.* **2004**, *126*, 5593–5600.

(93) Köhn, A.; Hättig, C. On the nature of the low-lying singlet states of 4-(dimethyl-amino) benzonitrile. *J. Am. Chem. Soc.* **2004**, *126*, 7399–7410.

(94) Kobayashi, R.; Amos, R. D. The application of CAM-B3LYP to the charge-transfer band problem of the zincbacteriochlorin–bacteriochlorin complex. *Chem. Phys. Lett.* **2006**, *420*, 106–109.

(95) Duchemin, I.; Deutsch, T.; Blase, X. Short-range to long-range charge-transfer excitations in the zincbacteriochlorin-bacteriochlorin complex: a Bethe-Salpeter study. *Phys. Rev. Lett.* **2012**, *109*, 167801.

(96) Yamaguchi, Y.; Yokomichi, Y.; Yokoyama, S.; Mashiko, S. Time-dependent density functional calculations of the Q-like bands of phenylene-linked free-base and zinc porphyrin dimers. *Int. J. Quantum Chem.* **2001**, *84*, 338–347.

(97) Yamaguchi, Y.; Yokoyama, S.; Mashiko, S. Strong coupling of the single excitations in the Q-like bands of phenylene-linked free-base and zinc bacteriochlorin dimers: A time-dependent density functional theory study. *J. Chem. Phys.* **2002**, *116*, 6541–6548.

(98) Blase, X.; Attaccalite, C. Charge-transfer excitations in molecular donor-acceptor complexes within the many-body Bethe-Salpeter approach. *Appl. Phys. Lett.* **2011**, *99*, 171909.

(99) Momeni, M. R.; Brown, A. Why do TD-DFT excitation energies of BODIPY/aza-BODIPY families largely deviate from experiment? Answers from electron correlated and multireference methods. *J. Chem. Theory Comput.* **2015**, *11*, 2619–2632.

(100) Hait, D.; Rettig, A.; Head-Gordon, M. Beyond the Coulson–Fischer point: characterizing single excitation CI and TDDFT for excited states in single bond dissociations. *Phys. Chem. Chem. Phys.* **2019**, *21*, 21761–21775.

(101) Filatov, M.; Huix-Rotllant, M. Assessment of density functional theory based ΔSCF (self-consistent field) and linear response methods for longest wavelength excited states of extended π-conjugated molecular systems. *J. Chem. Phys.* **2014**, *141*, 024112.

(102) Filatov, M. Description of electron transfer in the ground and excited states of organic donor–acceptor systems by single-reference and multi-reference density functional methods. *J. Chem. Phys.* **2014**, *141*, 124123.

(103) Marenich, A. V.; Cramer, C. J.; Truhlar, D. G.; Guido, C. A.; Mennucci, B.; Scalmani, G.; Frisch, M. J. Practical computation of electronic excitation in solution: vertical excitation model. *Chem. Sci.* **2011**, *2*, 2143–2161.

(104) Marenich, A. V.; Cramer, C. J.; Truhlar, D. G. Sorting out the relative contributions of electrostatic polarization, dispersion, and hydrogen bonding to solvatochromic shifts on vertical electronic excitation energies. *J. Chem. Theory Comput.* **2010**, *6*, 2829–2844.